Time-Dependent Quantum Dynamics Study of the Cl + HD Reaction†

ARTICLE *in* THE JOURNAL OF CHEMICAL PHYSICS · OCTOBER 2000

Impact Factor: 2.95 · DOI: 10.1021/jp0014115

3 AUTHORS, INCLUDING:

Hong-Ming Yin
Dalian Maritime University
39 PUBLICATIONS **509** CITATIONS

SEE PROFILE

Time-Dependent Quantum Dynamics Study of the Cl + HD Reaction†

Ben-Hui Yang, Hong-Ming Yin, and Ke-Li Han*

Center for Computational Chemistry, State Key Laboratory of Molecular Reaction Dynamics, Dalian Institute of Chemical Physics, Chinese Academy of Sciences, Dalian 116023, China

John Z. H. Zhang

Department of Chemistry, New York University, New York, New York 10003

Received: April 14, 2000; In Final Form: August 3, 2000

The dynamics of the Cl + HD reaction has been studied by means of time-dependent quantum wave packet calculations on the G3 and BW2 potential energy surfaces. Initial state-specific total reaction probabilities and integral cross sections are calculated, and the thermal rate constant is obtained. The good agreement was shown in the comparison of our integral cross sections with other quantum mechanics calculations on the same PES. The thermal rate constants on the G3 surface are close to the experiment findings. In the case of neglect of spin−orbit coupling in the ab initio calculations of the BW2 surface, the thermal rate constants on the surface are somewhat higher than the experimental measurement. When the spin−orbit coupling is taken into account, the thermal rate constants on the BW2 surface are close to the experiment as well.

I. Introduction

The reaction Cl + H_2 and its isotopic variants have played a key role during the development of gas-phase reaction dynamics. In recent years, decisive progress, both theoretical and experimental, have been made toward a precise knowledge of the Cl + H_2 reaction and its isotopic variants.[1−15] These reactions have been a prototypical three-atom reaction system in the field of molecular dynamics and have served as test cases for bimolecular reaction rate theory,[16] particularly transition state theory[17] and the theory of isotope effects that derived from it.[18] The isotope effects in reaction dynamics are kinetically interesting because they provide different dynamic view of the same potential energy surface (PES).

To date, impressive progress has been made in the constructing PES for the H_2Cl reaction system. In 1996, Allison et al.[3] presented one global potential energy surface called G3 by modifying GQQ surface of Schwenke et al.[19] The G3 PES is a significant step forward in quantitative modeling of the Cl + H_2 reaction and has already been used for a number of dynamical studies.[4−7,13−15] The rate constants from the quantum mechanics (QM)[4] and quasiclassical trajectory (QCT)[5] calculations showed a fairly general good agreement with the experimental, but tended to yield too high values at low temperatures. As pointed out by Allison et al.,[3] the theoretical rate constants are larger than the experimental measurement at the low temperatures might indicates that the collinear barrier given by the G3 PES is probably too thin and leads to more pronounced tunneling effects.

More recently, Bian et al.[9] presented a new, fully ab initio PES called BW2 for H_2Cl reaction system. An accurate quantum calculation has been performed by Manthe et al.[10] to investigate the thermal rate constant on the surface obtained by modifying the rate constants for the effect of the spin−orbit coupling on the barrier height. In contrast to the G3 PES, the exact QM reactive scattering calculations for Cl + HD on the BW2 PES predicted the large DCl/HCl branching ratios at low collisions energies correctly and in better agreement with the recent crossed molecule beam experiment measurement.[11]

The BW2 surface differs qualitatively from the G3 surface in several respects. First, in both the entrance and exit channels, the BW2 surface has long-range van der Waals minima which are absent in the LEPS-type G3 surface. Second, in the entrance channel, the BW2 surface is least repulsive for perpendicular (T-shaped) approach of Cl toward H_2 while the G3 surface is most repulsive for the T-shaped structure. The saddle point of the BW2 surface is located earlier in the entrance channel than that of the G3 surface while the barrier height of the BW2 surface (7.61kcal/mol) is very close to that of the G3 surface (7.88 kcal/mol). Also the effective barrier height by adding the zero point energies at the saddle and the asymptotic channel of the BW2 surface (4.03kcal/mol) is very close to that of the G3 surface (4.36kcal/mol). In addition, the BW2 imaginary frequency (1294*i* cm^{-1}) corresponding to the asymmetric stretch is substantially smaller than that (1520*i* cm^{-1}) of the G3 surface, indicating that the reaction barrier of the BW2 surface is thicker than that of the G3 surface.

On the experimental side, the infrared frequency-modulation measurements of absolute rate constants for Cl + HD reaction between 295 and 700K have been reported by Taatjes.[8] In addition, in ref 11 Skouteris et al presented the results of van der Waals interactions in the Cl + HD reaction in a crossed molecular beam experiment. They found a strong preference for the production of DCl in the HCl and DCl products by measuring the reaction excitation function for each of the two product channels.

Currently, time-dependent (TD) wave packet approach provides a competitive alternative to the time-independent (TID) approach for numerical solutions in gas-phase reactive scattering.[20−24] Efficient time-dependent methods for dynamical calculation have been developed for atom−diatom reaction[25−33] and diatom−diatom reaction.[34−41] In these approach, absorbing

† Part of the special issue "C. Bradley Moore Festschrift".

* Corresponding author. E-mail: klhan@ms.dicp.ac.cn.

10.1021/jp0014115 CCC: $19.00
Published on Web 10/10/2000

potentials V_p are employed to absorb the wave function to avoid boundary reflection of the wave function due to finite numerical grid.[42]

We report in the present work the results of TD wave packet calculation of total reaction probabilities and integral cross sections for Cl reacting with HD on both the G3 and BW2 surfaces. The thermal rate constants of HD are calculated by employing the uniform *J*-shifting method,[44,45] and a comparison with experimental measurement is provided.

This paper is organized as follows: section II gives a brief review of the quantum TD reactive dynamics used in the current study. The result of calculation and discussion of the result are given in sections III, and section IV concludes.

II. Quantum TD Reactive Dynamics

In this section we briefly outline the TD wave packet treatment for atom−diatom reaction dynamics. The reader is referred to ref 26 for more detailed discussions of the methodology. The Hamiltonian expressed in the reactant Jacobi coordinate for a given total angular momentum *J* can be written as

$$\mathrm{H} = -2\frac{\hbar^2}{2\mu_R}\frac{\partial^2}{\partial R^2} + \frac{(\mathbf{J}-\mathbf{j})^2}{2\mu_R R^2} + \frac{\mathbf{j}^2}{2\mu_r r^2} + V(\mathbf{r},\mathbf{R}) + h(r) \quad (1)$$

where **r** is the diatom internuclear vector, **R** is the vector jointing the center of mass of diatom to the atom. μ_r and μ_R are two corresponding reduced masses. **J** and **j**, respectively, represent the total angular momentum operator and the rotational angular momentum operator of diatom. $V(\mathbf{r}, \mathbf{R})$ is the interaction potential excluding the diatomic potential of diatom. The diatomic reference Hamiltonian $h(r)$ is defined as

$$h(r) = -\frac{\hbar^2}{2\mu_r}\frac{\partial^2}{\partial r^2} + V_r(r) \quad (2)$$

where $V_r(r)$ is a diatomic reference potential.

The time-dependent wave function satisfying the Schrödinger equation $i\hbar(\partial/\partial t)\Psi(t) = H\Psi(t)$ can be expanded in terms of the BF translational−vibrational−rotational basis defined using the reactant Jacobi coordinates as[26]

$$\Psi^{JM\epsilon}_{v_0, j_0, K_0}(\mathbf{R}, \mathbf{r}, t) = \sum_{n,v,j,K} F^{JM\epsilon}_{nvjK, v_0 j_0 K_0}(t) u_n^v(R)\phi_v(r)\, Y^{JM\epsilon}_{jK}(\hat{R}, \hat{r}) \quad (3)$$

where *n* is the translational basis label, *M* is the projection quantum number of *J* on the space-fixed *z* axis, (v_0, j_0, K_0) denotes the initial rovibrational state, and ϵ is the parity of the system defined as $\epsilon = (-1)^{j+L}$ with *L* being the orbital angular momentum quantum number. The definitions of various basis functions can be found elsewhere.[26]

The split-operator method[46] is employed to carry out the wave packet propagation. And the time-dependent wave function is absorbed at the edges of the grid to avoid boundary reflections.[42] The total reaction probability is obtained by evaluating the reactive flux.[26,35]

$$P_i^R(E) = \frac{\hbar}{\mu_r} Im\left[\left\langle \psi_{iE}^+ \middle| \delta(r - r_0)\frac{\partial}{\partial r} \middle| \psi_{iE}^+ \right\rangle\right] \quad (4)$$

where the dividing surface for flux calculation is chosen at $r = r_0$. The stationary wave function ψ_{iE}^+ is obtained through a Fourier transformation as described in ref 26.

After the reaction probabilities $P_i^R(E)$ have been calculated for all fixed angular momenta *J*, we can evaluate the reaction cross section for a specific initial state by simply summing the reaction probabilities over all the partial waves (total angular momentum *J*),

$$\sigma_{v_0 j_0}(E) = \frac{\pi}{k^2_{v_0 j_0}} \sum_J (2J+1) P^J_{v_0 j_0}(E) \quad (5)$$

where k_{n_0,j_0} is the wavenumber corresponding to the initial state at fixed collision energy *E*. In practice, reaction probabilities at only a limited number of total angular momentum values of *J* need to be explicitly calculated and probabilities for missing values of *J* are obtained through interpolation.

The reaction rate constant can be calculated using a uniform version[44,45] of the *J*-shifting approach.[47] The initial state-specific thermal rate constant in the uniform *J*-shifting scheme is given by

$$r'(T) = \sqrt{\frac{2\pi}{(\mu_R kT)^3}}\, Q^0(T) \sum_J (2J+1) e^{-B_J(T)J(J+1)/kT} \quad (6)$$

The shifting constant is determined by[45]

$$B_J(T) = \frac{kT}{J(J+1)} ln\left(\frac{Q^0}{Q^J}\right) \quad (7)$$

where *k* is the Boltzmann constant, *T* is the temperature, and Q^0 is a partition-like function defined as

$$Q^0 = \int P^0(E) \mathrm{e}^{-E/kT} \mathrm{d}E \quad (8)$$

and Q^J is similarly defined as

$$\mathrm{Q}^J = \int P^J(E) \mathrm{e}^{-E/kT} \mathrm{d}E \quad (9)$$

where $P^J(E)$ is the reaction probability for a total angular momentum *J* from a given initial state.

In practical applications of quantum dynamics, it is desirable to calculate the total reaction probability for more than two values of *J* in order to obtain more accurate rate constant.[45] Typically, using reaction probabilities evaluated at three values of *J* can yield very accurate rate constant.[45]

III. Results and Discussion

The time-dependent methodology described in section II was applied to study the Cl + HD reactive scattering on the G3 and BW2 surfaces, respectively. Below, we present and discuss the results (total reaction probabilities, integral cross sections, and rate constants).

Reaction Probabilities. The calculations for the Cl + HD reaction was carried out in the collision energy range [0.1,1.0]-eV, based on the two surfaces, G3 and BW2, respectively. To start, we consider the total reaction probabilities when HD is initially in its ground state. In Figure 1, we plot the total reaction probabilities as a function of collision (translational) energy from the initial ground state of the HD reactant for total angular momentum $J = 0$. As shown in Figure 1, near the threshold, the reaction probability obtained on the G3 surface are larger than that on BW2 surface. This results from several features of the BW2 surface which are different from the G3 surface. The G3 surface has no van der Waals well, and is most repulsive for perpendicular approach of the HD to Cl. In contrast to this, the BW2 surface is attractive at long distances, and has a minimum with a well depth of 0.5 kcal/mol for a T-shaped

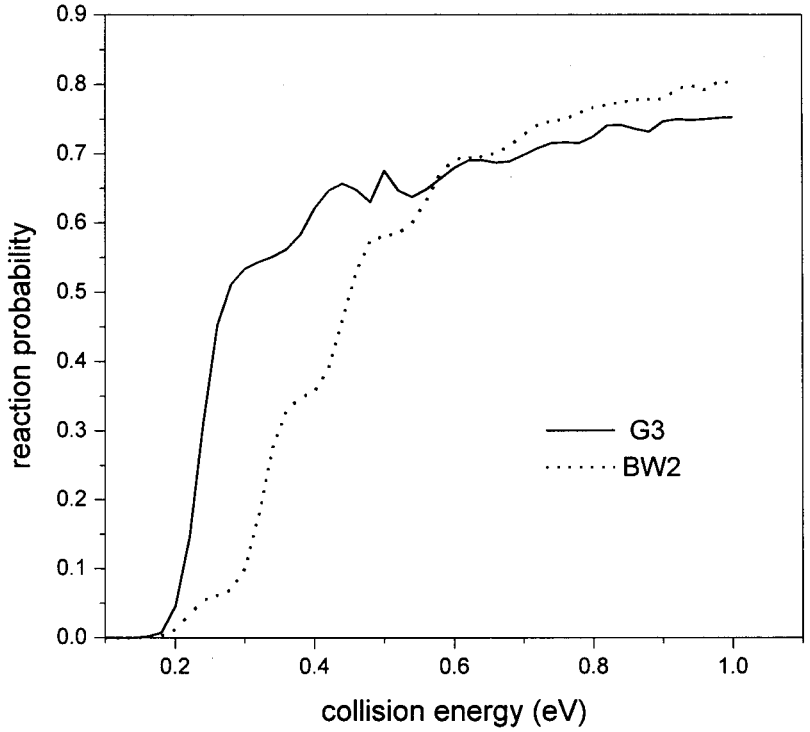

Figure 1. Total reaction probabilities for $J = 0$ from the ground state of the HD reactant for the Cl + HD reaction on the G3 and BW2 surfaces. The solid line is for the G3 surface, the dotted line is for the BW2 surface.

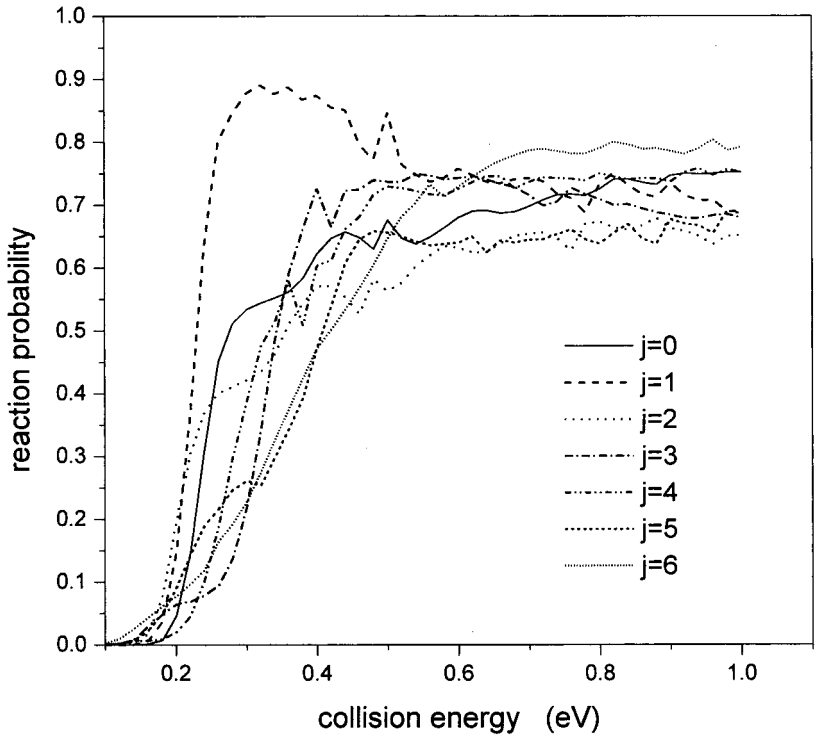

Figure 2. Total reaction probabilities of $J = 0$ for $j = 0-6$ on the G3 surface. Solid line is for $j = 0$, dashed line for $j = 1$, dotted line for $j = 2$, dashed−dotted line for $j = 3$, dashed−dotted−dotted line for $j = 4$, short dashed line for $j = 5$, and short dotted line for $j = 6$.

structure. Moreover, there is a more notable difference in the imaginary frequencies that the imaginary frequency on the BW2 surface is about 230 cm^{-1} lower than that on the G3 surface, indicating that the barrier of the BW2 surface is wider than that of the G3 surface. It is plausible that the relatively thinner barrier on the G3 surface enables easier barrier transmission by the system than the thicker barrier on the BW2 surface.

In addition to investigating the reaction probabilities for HD initially in its ground state for the G3 and BW2 potentials, we have calculated the energy resolved reaction probabilities with HD initially in the states ($v = 0, j = 1-6$) to show the rotational dependencies. The results for $J = 0$ are presented in Figures 2 and 3 on G3 and BW2 surfaces, respectively. As with the results reported in Figures 2 and 3, the increasing rotational excitation

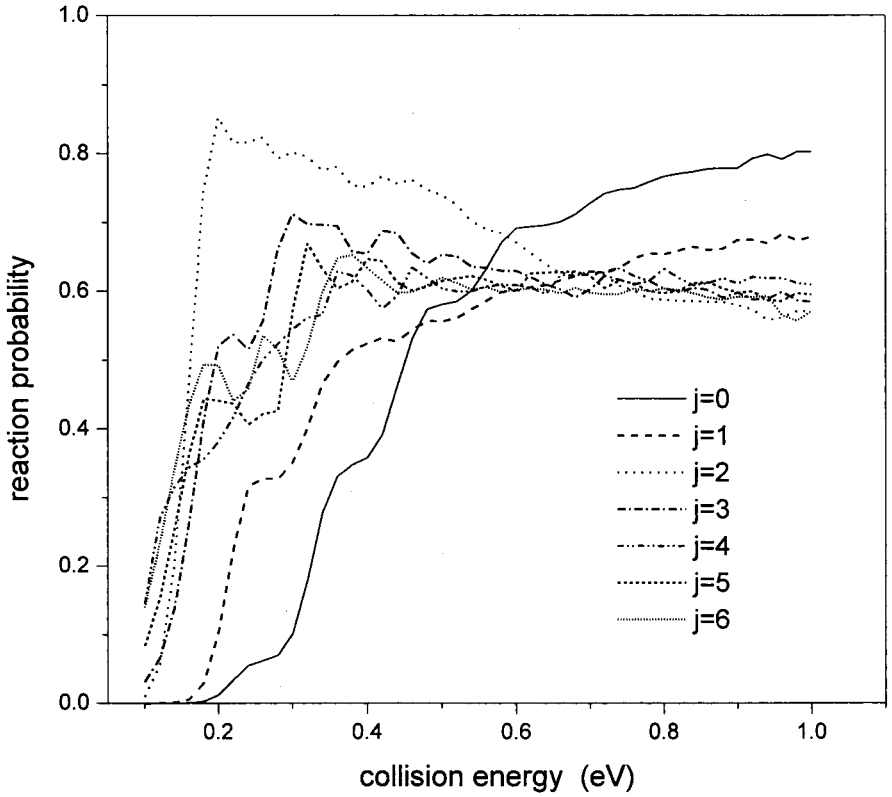

Figure 3. Total reaction probabilities of $J = 0$ for $j = 0-6$ on the BW2 surface. Solid line is for $j = 0$, dashed line for $j = 1$, dotted line for $j = 2$, dashed−dotted line for $j = 3$, dashed−dotted−dotted line for $j = 4$, short dashed line for $j = 5$, and short dotted line for $j = 6$.

of HD has visible effect on the reaction probability. For the G3 surface, Figure 2 shows that over the energy range of interest the $j = 1$ results are larger than those for $j = 0$, and near the threshold region the $j = 2$ results are larger than those of $j = 0$, whereas in the high energy region $j = 2$ gives the smaller results than $j = 0$. While the reaction probabilities of other rotational levels ($j = 3,...,6$) are different from $j = 1, 2$ as shown in Figure 2. Generally, the results of $j = 3,...,5$ are smaller than those of $j = 0$ in the low energy region, and present larger results than $j = 0$ in the high energy region. For the BW2 surface, as depicted in Figure 3, in general, the increasing rotational quantum number j, up to $j = 6$, results in the increasing of reaction probabilities in the low energy region.

Integral Cross Sections. In the present work, we have performed the calculations of the collision energy dependence of the integral cross sections for two initial rotational state ($j = 0$, 1, and 3) on both the G3 and BW2 surfaces, respectively. As done in ref 11, the reactant molecule is in its ground vibrational state ($v = 0$). With the use of the hyperspherical coordinate reaction scattering methods, Skouteris et al.[11] presented the exact quantum mechanical results of the reaction excitation functions (that is, the translational energy dependence of the cross section) for the Cl + HD ($v = 0$, 82%$j = 0$ +18%$j = 1$). Their calculations were carried out on the G3 and BW2 surfaces at 26 total energies between 0.35 and 0.60 eV, respectively. One can find that the theoretical results of ref 11 consist of absolute reaction cross sections for the Cl + HD → HCl + D and Cl + HD → DCl + H reactions. While, in our calculations, the integral reaction cross sections are calculated for reaction Cl + HD, to facilitate the comparison of our results with those of ref 11. The following steps are taken: (1) the cross sections corresponding to different product channels HCl and DCl in ref 11 are summed up to obtain the integral cross section δ_1 for the reaction Cl + HD; (2) as for our results, 82% of the integral cross section corresponding to initial rotational state $j = 0$ and 18% of that of initial rotational state $j = 1$ are summed up to yield δ_2, which will be compared with δ_1 directly.

Figures 4 and 5 depict the comparison of the our integral cross sections with those from ref 11 on the G3 and BW2 surfaces, respectively. It is observed that there is a very good agreement between the TD wave packet calculation in this paper and hyperspherical coordinate reaction scattering calculation from ref 11.

Also, in Figure 6 we plot the integral cross sections on the G3 and BW2 surfaces as a function of collision energy from the initial ground state of the HD reactant. Comparison show that the cross sections from the BW2 surface are much smaller than those on the G3 PES. This result is obviously expected based on the energy dependence of individual reaction probabilities on two surfaces discussed above.

In addition, to show the reagents' rotational excitation effect on the reactivity we present in Figures 7 and 8 the integral cross sections for initial rotational states $j = 0$, $j = 1$, and $j = 3$ on the G3 and BW2 surfaces, respectively. It can be found from Figure 7 that, for the G3 surface, an increase of the HD rotational quantum number j results in lower values of the integral cross section at a given collision energy, that is to say, the effect of reagent rotation is negative on the G3 surface. While the effect of reagent rotation is positive on the BW2 surface, Figure 8 shows that the integral cross section increases with the increasing of rotational quantum number j. The reason is that, the G3 surface is collinearly constrained throughout its entrance valley, the initial rotation would hinder the reactants into the cone of acceptance steered by the forces outside the barrier in absence of rotation, leading to a decline of cross section with j for the first rotational quantum, thus diminishing the possible orienting effect of the potential energy surface.[14] However, the BW2

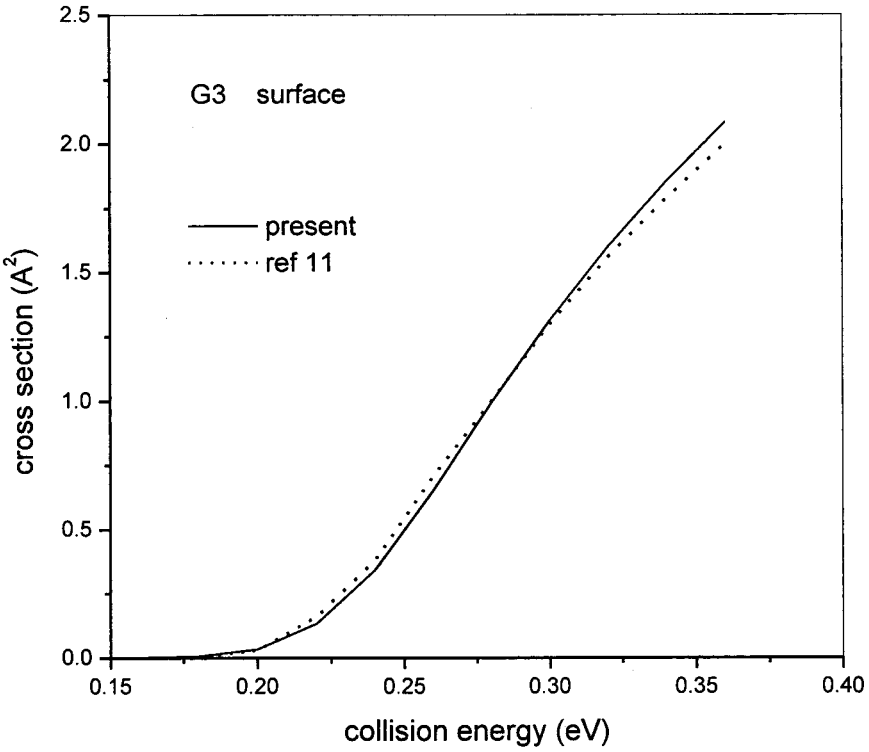

Figure 4. Integral reaction cross sections (angstrom squared) on the G3 surface as a function of collision energy for the Cl + HD ($v = 0$, 82%$j = 0$ +18%$j = 1$) reaction. Solid line is for the present calculation, dotted line is for the quantum mechanical calculation from ref 11.

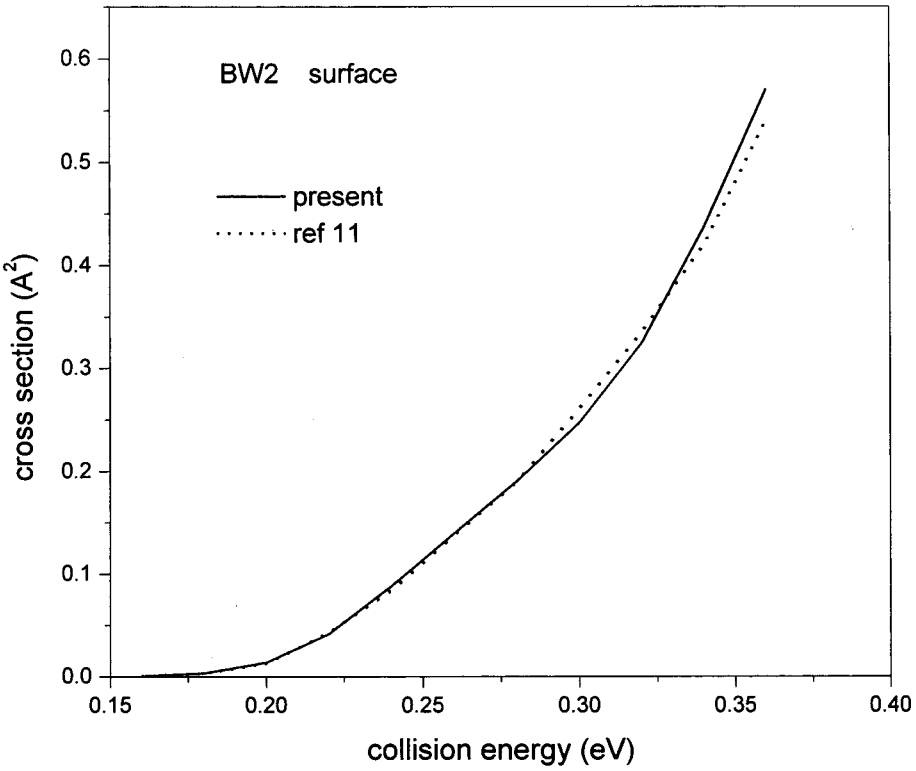

Figure 5. Integral reaction cross sections (angstrom squared) on the BW2 surface as a function of collision energy for the Cl + HD ($v = 0$, 82%$j = 0$ +18%$j = 1$) reaction. Solid line is for the present calculation; dotted line is for the quantum mechanical calculation from ref 11.

surface has a Cl−HD van der Waals well with a nonlinear equilibrium geometry,[9,11] and the van der Waals interactions are not confined to the well region but persist for some distance into the side of the reaction barrier. When the HD is in the low rotational excitation, the van der Waals interactions deflect trajectories away from the collinear transition state saddle point. When the HD is in the high rotational states, the van der Waals interactions are weaker, then trajectories with more rapid HD rotation are not deflected so strongly by the van der Waals forces.[11]

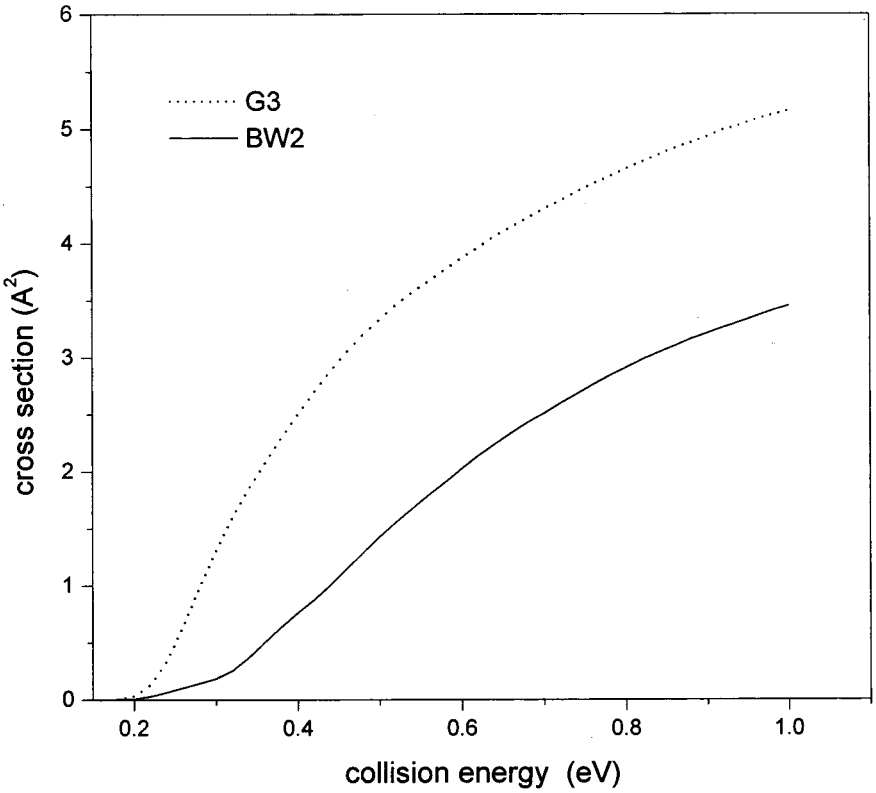

Figure 6. Integral reaction cross sections (angstrom squared) on the G3 and BW2 surfaces as a function of collision energy for the Cl + HD reaction from the initial ground state. Solid line is for the BW2 surface, dotted line is for the G3 surface.

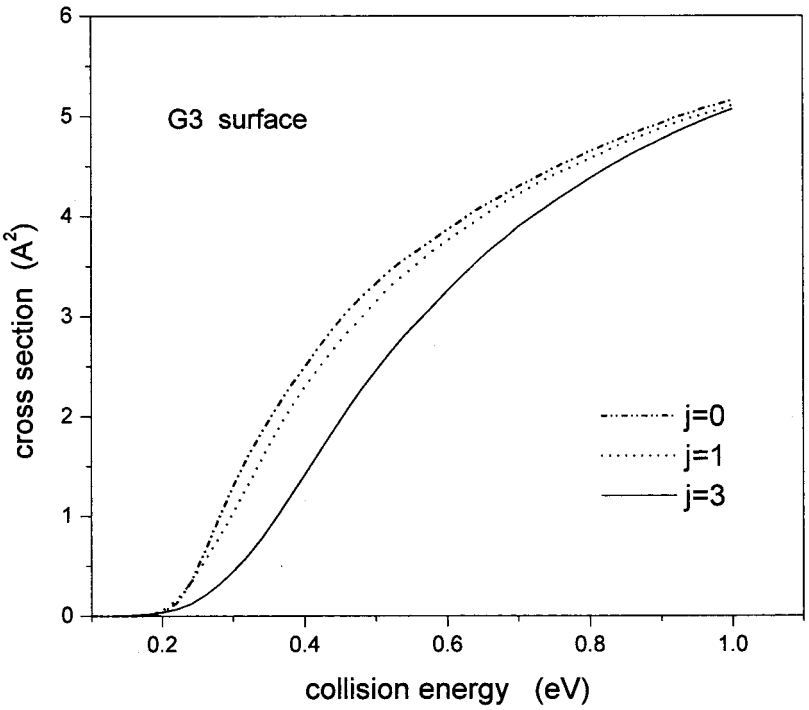

Figure 7. Integral reaction cross sections (angstrom squared) on the G3 surface for the initial rotational states $j = 0$, 1, and 3. Dash dot dotted line is for $j = 0$, dotted line is for $j = 1$ and solid line is for $j = 3$.

Rate Constants. Thermal rate constants were calculated for the Cl + HD reaction between 200 and 550K. In our calculation we only consider the zeroth vibrational level for different initial rotational states $j = 0-6$ of HD, which permits the calculation of the thermal rate constants in the range of temperatures between 200 and 550 K.

We calculated the reaction rate constants r_j for the initial states ($v = 0, j = 0-6$) of HD by using the uniform J-shift approach.[45] Equation 7 is used to generate the optimized shifting constant $B(T)$ for each adjacent pair of J values, and the shifting constants are defined:

$$B_i(T) = \frac{kT}{J_{i+1}(J_{i+1}+1)} \ln\left(\frac{Q^{J_i}}{Q^{J_i+1}}\right)_{(i=1,2,\ldots,)} \quad (10)$$

According to the thermal distribution of the rotational levels,[48]

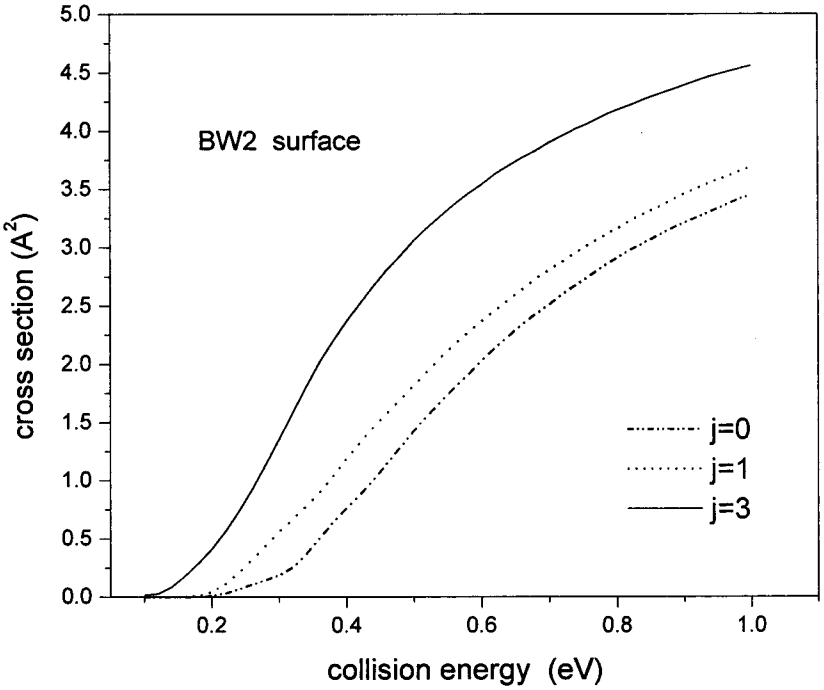

Figure 8. Integral reaction cross sections (angstrom squared) on the BW2 surface for the initial rotational states $j = 0$, 1, and 3. The dash dot dotted line is for $j = 0$, the dotted line is for $j = 1$ and the solid line is for $j = 3$.

the rate constant of HD at the temperature T can be expressed as

$$r(T) = \sum_{j=0} \frac{r_j}{Q_r}(2j+1)e^{-Bj(j+1)hc/kT} \quad (11)$$

in which Q_r is[48]

$$Q_r = 1 + 3e^{-2Bhc/kT} + 5e^{-6Bhc/kT} + ... \quad (12)$$

where B is the rotational constant of HD, k is Boltzmann constant, h is Planck's constant, and c is the velocity of light in a vacuum.

As mentioned by Mielke et al.,[4] the ground electronic state $^2P_{3/2}$ of the Cl atom is 4-fold degenerate and only two states correlate adiabatically with the product. So a statistical weight factor should be included in order to make comparison of theoretical result with experimental measurement. This factor is given by[4]

$$B'(T) = \frac{2}{4 + 2\exp\{-\Delta E/kT\}} \quad (13)$$

where ΔE is the energy splitting between the two fine structure states of Cl, $^2P_{1/2}$ and $^2P_{3/2}$, taken as 881 cm^{-1}.

Similar to the reagent's rotational effect on the integral cross sections plotted in Figures 7 and 8, we also show the effect of reagent rotation on the rate constant, the rate constants r_j for different initial rotational states j ($j = 0$, 1, and 3) on the G3 and BW2 surfaces in Figures 9 and 10, respectively. For a given temperature, from Figure 9 one can see that the rate constants on the G3 surface decrease with rotational excitation. However, as depicted in Figure 10, for a given temperature, the rate constants on the BW2 surface increase with rotational excitation. This is in accordance with the integral cross section behavior displayed by Figures 7 and 8.

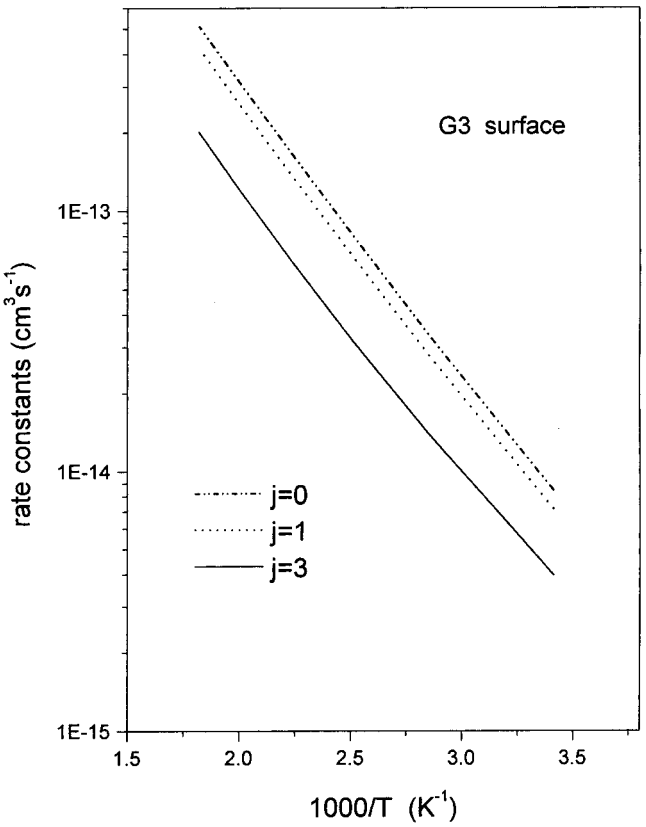

Figure 9. Arrhenius plot of our theoretical rate constants on the G3 surface for the initial rotational states $j = 0$, 1, and 3. The dash dot dotted line is for $j = 0$, the dotted line is for $j = 1$, and the solid line is for $j = 3$.

However, Manthe et al.[10] proposed that the BW2 surface does not include the spin−orbit (SO) interaction. Thus, the potential energy surface correlates asymptotically to the average energy of the $^2P_{1/2}$ and $^2P_{3/2}$ states of the chlorine atom. Consequently,

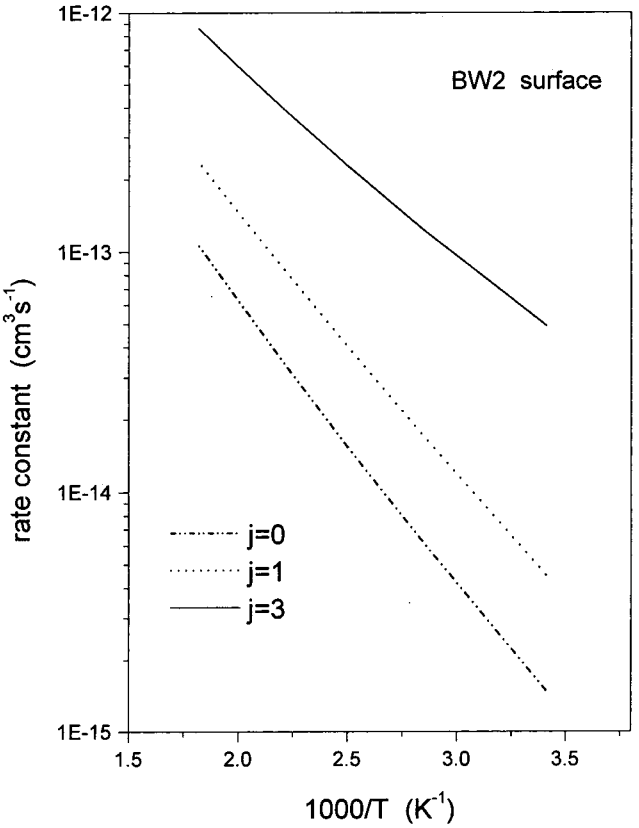

Figure 10. Arrhenius plot of our theoretical rate constants on the BW2 surface for the initial rotational states $j = 0$, 1, and 3. The dash dot dotted line is for $j = 0$, the dotted line is for $j = 1$, and the solid line is for $j = 3$.

the electronic part of the partition function of the reactants has to be taken as

$$Q_r^{elec}(T) = 2\exp\left(\frac{1}{3}\frac{\Delta E}{kT}\right) + \exp\left(-\frac{2}{3}\frac{\Delta E}{kT}\right) \qquad (14)$$

where ΔE is the SO splitting of the chlorine atom. This electronic partition function effectively lowers the asymptotic potential energy of the reactants by $^1/_3\Delta E = 0.84$ kcal/mol. Since at the barrier the effect of SO is almost negligible, the effective barrier height will be increased by about this value.

The comparison of the thermal rate constants $k(T)$ obtained from 200 to 550 K between our calculations on the G3 and BW2 surfaces and the experiment from ref 8 is given in Figure 11. Figure 11 shows that the present results on the G3 surface are in agreement with experiment at the lower temperatures and are somewhat larger than the experimental findings at the higher temperatures.

In general the rate constants modified by using eq 13 on the BW2 surface, the dotted line in Figure 11, are larger than the experimental measurements. However, the rate constants modified by using eq 14 which is displayed in the solid line in Figure 11, in general, are in agreement with the experiment findings, but the results are somewhat larger than the experiment at higher temperatures and smaller than the experiment at lower temperatures.

IV. Conclusion

We have carried out the time-dependent quantum dynamics calculations for the Cl + HD reaction. Initial state-selected total reaction probabilities for total angular momentum J are computed on the G3 and BW2 potentials. Because of the different topology of these two surfaces, the dynamics on them is quite different. Besides the difference in overall topology on two surfaces, the barrier on the G3 surface is thinner than that on the BW2 surface and may be responsible for the enhanced reaction probability on the G3 surface at the threshold region. The calculated quantum integral cross sections are in good agreement with those obtained using hyperspherical coordinate reaction scattering methods on the G3 and BW2 surfaces. The effect of reagent rotation on the reactivity on the G3 surface is negative, while the effect of reagent rotation on the reactivity on the BW2 surface is positive. The thermal rate constants on the G3 surface are close to the experiment findings. In the case of neglect of spin−orbit coupling in the ab initio calculations of the BW2 surface, the thermal rate constants on the surface are somewhat higher than the experimental measurement. When the spin−orbit coupling is taken into account, the thermal rate constants on the BW2 surface are close to the experiment as well.

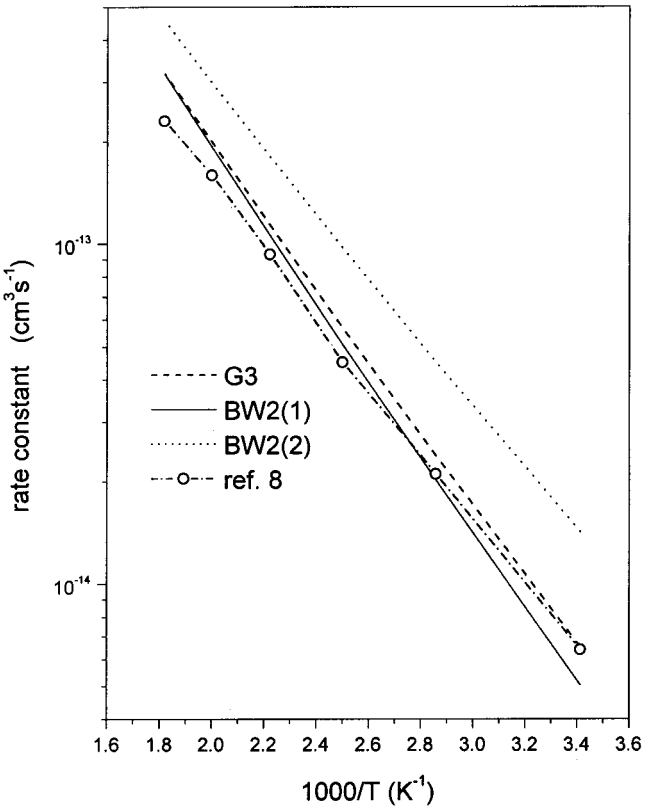

Figure 11. Arrhenius plot of theoretical (on the G3 and BW2 surfaces) and experimental rate constants for the Cl + HD reaction. The dashed line is the present calculation on the G3 surface, the dotted line is the present calculation modified by using eq 13 on the BW2 surface, and the solid line is the present calculation modified by using eq 14 on the BW2 surface. and the dashed−dotted line with open symbol is experimental result from ref 8.

Acknowledgment. This work is supported by the Outstanding Young Scientist Foundation of China from NSFC. Benhui Yang also gratefully acknowledges the support of K. C.Wong Education Foundation, Hong Kong.

References and Notes

(1) Miller, J. C.; Gordon, R. J. *J. Chem. Phys.* **1983**, *79*, 1252.
(2) Kumaran, S. S.; Lim, K. P.; Michael, J. A. *J. Chem. Phys.* **1994**, *101*, 9487.
(3) Allison, T. C.; Lynch, G. C.; Truhlar, D. G. *J. Phys. Chem.* **1996**, *100*, 13575.

(4) Mielke, S. L.; Allison, T. C.; Truhlar, D. G.; Schwenke, D. W. *J. Phys. Chem.* **1996**, *100*, 13588.
(5) Aoiz, F. J.; Banares, L. *J. Phys. Chem.* **1996**, *100*, 18108.
(6) Alagia, M.; Balucani, N.; Cartechini, L.; Casavecchia, P.; van Kleef, E. H.; Volpi, G. G.; Aoiz, F. J.; Banares, L.; Schwenke, D. W.; Allison, T. C.; Mielke, S. L.; Truhlar, D. G. *Science* **1996**, *273*, 1519.
(7) Wang, H.; Thompson, W. H.; Miller, W. H. *J. Chem. Phys.* **1997**, *107*, 7194.
(8) Taatjes, C. A. *Chem. Phys. Lett.* **1999**, *306*, 33.
(9) Bian, W.; Werner, H.-J. *J. Chem. Phys.* **2000**, *112*, 220.
(10) Manthe, U.; Bian, W.; Werner, H.-J. *Chem. Phys. Lett.* **1999**, *313*, 647.
(11) Skouteris, D.; Manolopoulos, D. E.; Bian, W.; Werner, H.-J.; Lai, L.-H.; Liu, K. *Science* **1999**, *286*, 1713.
(12) Lee, S.-H.; Lai, L.-H.; Liu, K. *J. Chem. Phys.* **1999**, *110*, 8229.
(13) Srinivasan, J.; Allison, T. C.; Schwenke, D. G.; Truhlar, D. G. *J. Phys. Chem. A* **1999**, *103*, 1487.
(14) Alagia, M.; Balucani, N.; Cartechini, L.; Casavecchia, P.; Volpi, G. G.; Aoiz, F. J.; Banares, L.; Allison, T. C.; Mielke, S. L.; Truhlar, D. G. *Phys. Chem. Chem. Phys.* **2000**, *2*, 599.
(15) Kandel, S. A.; Alexander, A. J.; Kim, Z. H.; Zare, R. N.; Aoiz, F. J.; Banares, L.; Castillo, J. F.; Rabanos, V. S. *J. Chem. Phys.* **2000**, *112*, 670.
(16) Weston, R. E., Jr. *J. Phys. Chem.* **1979**, *83*, 61.
(17) Wheeler, A.; Topley, B.; Eyring, H. *J. Chem. Phys.* **1936**, *4*, 178.
(18) Bigeleisen, J.; Klein, F. S.; Weston, R. E., Jr.; Wolfsberg, M. *J. Chem. Phys.* **1959**, *30*, 1340.
(19) Schwenke, D. W.; Tucker, S. C.; Steckler, B.; Brown, F. B.; Lynch, G. C.; Truhlar, D. G.; Garrett, B. C. *J. Chem. Phys.* **1989**, *90*, 3110.
(20) McCullough E. A.; Wyatt, R. E. *J. Chem. Phys.* **1971**, *54*, 3578.
(21) Kulander, K. C. *J. Chem. Phys.* **1978**, *69*, 5064.
(22) Kosloff, R. *J. Phys. Chem.* **1988**, *92*, 2087.
(23) Zhang, Z. H.; Kouri, D. J. *Phys. Rev. A* **1986**, *34*, 2687.
(24) Neuhauser, D.; Baer, M.; Judson, R. S.; Kouri, D. J. *J. Chem. Phys.* **1989**, *90*, 5882; *Chem. Phys. Lett.* **1990**, *169*, 372.
(25) Neuhauser, D.; Baer, M.; Judson, R. S.; Kouri, D. J. *J. Chem. Phys.* **1990**, *93*, 312. Judson, R. S.; Kouri, D. J.; Neuhauser, D.; Baer, M. *Phys. Rev. A* **1990**, *42*, 351.
(26) Zhang, D. H.; Zhang, J. Z. H. *J. Chem. Phys.* **1994**, *101*, 3671. Dai, J.; Zhang, J. Z. H. *J. Phys. Chem.* **1996**, *100*, 6898.
(27) Gogtas, F.; Balint-Kurti, G. G.; Offer, A. R. *J. Chem. Phys.* **1996**, *104*, 7927.
(28) Zhu, W.; Wang, D. Y.; Zhang, J. Z. H. *Theor. Chem. Acta.* **1997**, *96*, 31.
(29) Meijer, A. J. H. M.; Goldfield, E. M. **1998**, *108*, 5404.
(30) Gray, S. K.; Balint-Kurti, G. G. *J. Chem. Phys.* **1998**, *108*, 950.
(31) Russell, C. L.; Manolopoulos, D. E. *J. Chem. Phys.* **1999**, *110*, 177.
(32) Zhang, Y. C.; Zhan, L. X.; Zhang, Q. G.; Zhu, W.; Zhang, J. Z. H. *Chem. Phys. Lett.* **1999**, *300*, 27.
(33) Wang, L.; Kalyanaraman, C.; McCoy, A. B. *J. Chem. Phys.* **1999**, *110*, 11221.
(34) Zhang, D. H.; Zhang, J. Z. H. *J. Chem. Phys.* **1993**, *99*, 5615; *J. Chem. Phys.* **1994**, *100*, 2697.
(35) Zhang, D. H.; Zhang, J. Z. H. *J. Chem. Phys.* **1994**, *101*, 1146.
(36) Neuhauser, D. *J. Chem. Phys.* **1994**, *100*, 9272.
(37) Zhang, D. H.; Zhang, J. Z. H. *Chem. Phys. Lett.* **1995**, *232*, 370. Zhang, D. H.; Zhang, J. Z. H.; Zhang, Y.; Wang, D.; Zhang, Q. *J. Chem. Phys.* **1995**, *105*, 7400. Zhang, Y.; Zhang, D.; Li, W.; Zhang, Q.; Wang, D.; Zhang, D. H.; Zhang, J. Z. H. *J. Phys. Chem.* **1995**, *99*, 16824. Zhang, D. H.; Zhang, J. Z. H. *J. Chem. Phys.* **1995**, *103*, 6512.
(38) Zhu, W.; Dai, J.; Zhang, J. Z. H. *J. Chem. Phys.* **1996**, *105*, 4881. Dai, J.; Zhu, W.; Zhang, J. Z. H. *J. Phys. Chem.* **1996**, *100*, 13901.
(39) Zhang, D. H.; Light, J. C. *J. Chem. Phys.* **1996**, *104*, 4544. Zhang, D. H.; Light, J. C. *J. Chem. Phys.* **1996**, *105*, 1291.
(40) Zhu, W.; Zhang, J. Z. H.; Zhang, Y. C.; Zhang, Y. B.; Zhan, L. X.; Zhang, S. L. *J. Chem. Phys.* **1998**, *108*, 3509. Zhu, W.; Zhang, J. Z. H.; Zhang, D. H. *Chem. Phys. Lett.* **1998**, *292*, 46.
(41) Zhang, D. H.; Light, J. C. *J. Chem. Phys.* **1997**, *106*, 551. Zhang, D. H.; Light, J. C.; Lee, S. Y. *J. Chem. Phys.* **1998**, *109*, 79.
(42) Neuhauser, D.; Baer, M. 1989 91, 4651. Neuhauser, D.; Baer, M.; Kouri, D. J. *J. Chem. Phys.* **1990**, *93*, 2499.
(43) Zhang, D. H.; Zhang, J. Z. H. *J. Chem. Phys.* **1994**, *101*, 3671.
(44) Mielke, S. L.; Lynch, G. C.; Truhlar, D. G.; Schwenke, D. W. *J. Phys. Chem.* **1994**, *98*, 8000.
(45) Zhang, D. H.; Zhang, J. Z. H. *J. Chem. Phys.* **1999**, *110*, 7622.
(46) Fleck, J. A. Jr.; Morris, J. R.; Feit, M. D. *Appl. Phys.* **1976**, *10*, 129.
(47) Sun, Q.; Bowman, J. M.; Schatz, G. C.; Sharp, J. R.; Connor, J. N. L. *J. Chem. Phys.* **1990**, *92*, 1677. Bowman, J. M. *J. Phys. Chem.* **1991**, *95*, 4960.
(48) Herzberg, G. *Molecular Spectra and Molecular Structure*, 2nd ed.; Van Nostrand: New York, 1957; Vol. 1, p 122.